Plant Physiology and Biochemistry 118 (2017) 449–459

Contents lists available at ScienceDirect

Plant Physiology and Biochemistry

journal homepage: www.elsevier.com/locate/plaphy

Research article

Physiological, vascular and nanomechanical assessment of hybrid poplar leaf traits in micropropagated plants and plants propagated from root cuttings: A contribution to breeding programs

Jaroslav Ďurkovič [a, *], Hana Husárová [a], Lucia Javoříková [a], Ingrid Čaňová [a], Miriama Šuleková [b], Monika Kardošová [b], Ivan Lukáčik [c], Miroslava Mamoňová [d], Rastislav Lagaňa [d]

[a] Department of Phytology, Technical University, T.G. Masaryka 24, 960 53 Zvolen, Slovak Republic
[b] Department of Integrated Forest and Landscape Protection, Technical University, T.G. Masaryka 24, 960 53 Zvolen, Slovak Republic
[c] Department of Silviculture, Technical University, T.G. Masaryka 24, 960 53 Zvolen, Slovak Republic
[d] Department of Wood Science, Technical University, T.G. Masaryka 24, 960 53 Zvolen, Slovak Republic

ARTICLE INFO

Article history:
Received 14 March 2017
Received in revised form
10 July 2017
Accepted 13 July 2017
Available online 13 July 2017

Keywords:
Cell wall nanomechanics
Chlorophyll *a* fluorescence
Dissipation energy
Transpiration
Vascular architecture
Water-use efficiency

ABSTRACT

Micropropagated plants experience significant stress from rapid water loss when they are transferred from an in vitro culture to either greenhouse or field conditions. This is caused both by inefficient stomatal control of transpiration and the change to a higher light intensity and lower humidity. Understanding the physiological, vascular and biomechanical processes that allow micropropagated plants to modify their phenotype in response to environmental conditions can help to improve both field performance and plant survival. To identify changes between the hybrid poplar [*Populus tremula* × (*Populus* × *canescens*)] plants propagated from in vitro tissue culture and those from root cuttings, we assessed leaf performance for any differences in leaf growth, photosynthetic and vascular traits, and also nanomechanical properties of the tracheary element cell walls. The micropropagated plants showed significantly higher values for leaf area, leaf length, leaf width and leaf dry mass. The greater leaf area and leaf size dimensions resulted from the higher transpiration rate recorded for this stock type. Also, the micropropagated plants reached higher values for chlorophyll *a* fluorescence parameters and for the nanomechanical dissipation energy of tracheary element cell walls which may indicate a higher damping capacity within the primary xylem tissue under abiotic stress conditions. The performance of the plants propagated from root cuttings was superior for instantaneous water-use efficiency which signifies a higher acclimation capacity to stressful conditions during a severe drought particularly for this stock type. Similarities were found among the majority of the examined leaf traits for both vegetative plant origins including leaf mass per area, stomatal conductance, net photosynthetic rate, hydraulic axial conductivity, indicators of leaf midrib vascular architecture, as well as for the majority of cell wall nanomechanical traits. This research revealed that there were no drawbacks in the leaf physiological performance which could be attributed to the micropropagated plants of fast growing hybrid poplar.

1. Introduction

The production of biomass crops, capable of fast growth, high yields and resilient to global warming, is a new challenge for the current plant breeding programs. Fast growing woody plants, such as poplars with a low lignin content, have been highlighted as a superior lignocellulosic biomass. By fermenting their carbohydrates they can be used successfully as a substrate in an integrated biorefinery for the production of second-generation biofuels and other chemicals (Sannigrahi and Ragauskas, 2010; Stolarski et al., 2015). The genus *Populus* comprise a host of species that are adaptable to multiple environmental stressors (Quinn et al., 2015). Interspecific hybrid poplars are rated among the most promising tree species for

* Corresponding author.
E-mail address: jaroslav.durkovic@tuzvo.sk (J. Ďurkovič).

http://dx.doi.org/10.1016/j.plaphy.2017.07.012
0981-9428/

energy generation due to a minimal requirement for fertilizer and an ability to grow on marginal infertile lands. Grey poplar (*Populus* × *canescens*) originates from the spontaneous hybridization between white poplar (*P. alba*) and aspen (*P. tremula*). This taxon grows best in damp ground, near rivers and water meadows, but it is also tolerant to oscillations in underground water levels and is capable of growth in either acidic or heavy clay soil. All of these attributes make it a very promising tree not only for phytoremedation of metal-contaminated soils and for commercial planting under the current constraints of global warming, but also, as a parental species for artificial hybridization along with other poplar clones to create new genotypes with an altered content of cell wall components (Bojarczuk et al., 2015; Ďurkovič et al., 2013; Zemleduch-Barylska and Lorenc-Plucińska, 2015). Current breeding strategies, that involve grey poplar hybrids as a feedstock, are aimed at achieving both a higher saccharification performance associated with an increased bioethanol yield and the utilization of resilient and perspective clones in the pulp and paper industry (Kaňuchová and Ďurkovič, 2013; Kučerová et al., 2016).

Understanding the physiological, vascular and biomechanical processes that allow micropropagated plants to modify their phenotype in response to environmental conditions can help to improve both field performance and plant survival. Micropropagated plants experience significant stress from rapid water loss when they are transferred from an in vitro culture to either greenhouse or field conditions. This is caused both by inefficient stomatal control of transpiration and the change to a higher light intensity and lower humidity which thereby requires the rapid development of survival mechanisms based on environmentally-induced shifts in phenotype (Osório et al., 2013). Leaves must now produce a photoassimilate which they formerly imported from the culture medium. This requirement involves modifying the photosynthetic apparatus to maintain its efficiency under a varying light energy load and to alleviate the damaging effects of environmental extremes (Osório et al., 2012; Savitch et al., 2000). The success of in vitro propagation as a source of material for reforestation or for the establishment of commercial plantations and orchards therefore depends on efficient transplantation protocols that ensure high survival rates and allow the micropropagated plants to become established in their new environment (Hazarika, 2006). Field assessment of gas exchange will provide information about stomatal control of net photosynthetic rate, transpiration and water-use efficiency (Ďurkovič et al., 2016; Osório et al., 2012). The photosynthetic apparatus is a conservative element within the plant cell, and its reaction centres have low specific characterization, but the features (size, pigment composition) of the antenna complexes are highly variable and specific to different groups of plant species (Kirova et al., 2009). In recent studies, chlorophyll *a* fluorescence has been used as a tool for taxonomic classification and physiological segregation of plant species (Ďurkovič et al., 2014; Pollastrini et al., 2016). Salvatori et al. (2014) demonstrated that a multivariate statistical analysis of chlorophyll *a* fluorescence parameters allows the discrimination of plant species according to their respective functional groups. Differences among taxa derive from specific strategies for the use and conservation of energy, and from interactions between genotypes and their environment. As shown previously, differences in chlorophyll *a* fluorescence yields may also reflect intraclonal and intraspecific variation in relation to the plant origin (Ďurkovič et al., 2010, 2016).

The mechanical properties of the cellular microenvironment, notably its rigidity and stiffness, possess a regulatory role for a variety of cellular responses including adhesion, migration, shape and division (Dufrêne et al., 2013; Janmey et al., 2009). For the cell walls of xylem tissue, quantifications of modulus of elasticity (MOE), adhesion and cell wall deformation play a key role in the assessment of the material stiffness, toughness and its adhesive properties (Ďurkovič et al., 2016). Nanoindentation is one method applied to the measurement of local mechanical properties of plant cell walls at the submicron level (Eder et al., 2013; Gindl et al., 2004). However, the spatial resolution of this technique is quite low. Atomic force microscopy (AFM), on the other hand, allows a much higher lateral spatial resolution than that of nanoindentation (Arnould and Arinero, 2015), as its scanning probes have more pointed angles than those provided by the tools of the indenters in nanoindentation. Nanoscale imaging by AFM provides valuable information concerning the cellulosic architectural structures (Ding et al., 2016; Zhou et al., 2014). Recent developments in PeakForce quantitative nanomechanical mapping (PeakForce QNM) have optimized this new AFM technique to a point where it enables high-resolution imaging of woody plant cell walls, so that the maps extracted from the arrays of force-distance curves provide crucial information on the nanomechanical properties of lignified cell walls (Ďurkovič et al., 2016; Ren et al., 2015).

In this study we focused on the verification of leaf physiological performance in micropropagated plants of hybrid poplar grown under field conditions when compared with plants propagated conventionally from root cuttings. The objectives for this study were: 1) to determine whether or not in vitro propagation technique compromises the performance of the micropropagated plants in leaf growth, gas exchange, chlorophyll *a* fluorescence yields, and vascular architecture; 2) to find possible differences between the examined stock types with respect to the nanomechanical properties of tracheary element cell walls, which could reveal any mechanical advantages for either stock type when using multiparametric quantitative imaging of force-distance curve-based PeakForce QNM; and 3) to identify correlations among the examined traits that could contribute to the leaf physiological performance of hybrid poplar plants in relation to the technique of vegetative propagation.

2. Materials and methods

2.1. Plant material, study site and sampling

The experiments were conducted on clonally micropropagated plants and plants propagated from root cuttings of the hybrid poplar clone T-14 [*Populus tremula* L. 70 × (*Populus* × *canescens* (Ait.) Sm. 23)]. This clone shows a decreased lignin content (17.37%) and a higher cellulose content (47.33%) compared to that of the reference clone *P.* × *euramericana* 'I-214', predominantly planted in Slovak poplar plantations (Kačík et al., 2012). The procedures of in vitro micropropagation through axillary and adventitious shoot formation from the sprouting axillary buds and the acclimatization to an ex vitro environment have previously been described in detail (Kaňuchová and Ďurkovič, 2013). For leaf trait comparisons, the counterparts of the micropropagated plants were derived from root cuttings having a length of approximately 30 cm. Both the root cuttings and the axillary buds originated from identical donor plants, more than 30 years of age. One-year-old plants propagated either by in vitro tissue culture or from root cuttings of a uniform size were selected and then planted in the experimental field plot at the Arboretum Borová hora, Slovakia (lat. 48°35′N, long. 19°08′E, altitude 297 m). Proper care was taken during planting to avoid any damage to the root system. The planting holes were dug with a spacing of 3 × 3 m. No post-planting treatments such as irrigation or fertilization were applied. The climate of the area is characterized by a mean annual temperature of 6.4 °C, a mean annual precipitation of 532 mm, and a mean precipitation of 315 mm in the growing season. The main soil creative substrates are slope loams of tufa materials with an admixture of loess loam. The experiments

were conducted on eight randomly chosen healthy plants per stock type. Measurements were performed on fully expanded leaves in the sixth growing season following planting. Scanning electron microscopy images of the plant leaf material used in this study are presented in Fig. 1a–d.

2.2. Leaf growth

Leaf growth characteristics were assessed on the third fully expanded leaf from the apex that was sampled from 5-leaved current-year shoots. Leaf sizes (area, length, width) were measured with an LI-3000A leaf area meter (LI-COR, Lincoln, NE, USA). Leaf slenderness was calculated as the ratio between leaf length and leaf width. Leaves were dried at 65 °C for 72 h, then weighed, and leaf dry mass was determined. Leaf mass per area (LMA) was calculated as the ratio between leaf dry mass and leaf area. Measurements were performed on five sun leaves per plant, one measurement per leaf. The experiments were repeated twice.

2.3. Leaf histology

Midrib sections (0.4 × 0.4 cm), excised from the leaf base, were fixed in 5% (v/v) glutaraldehyde in a 0.1 M cacodylate buffer at pH 7.0, dehydrated in ethanol and propylene oxide, and embedded in Spurr embedding medium. Cross-sections, approximately 1.5 μm thick, were cut using a Leica RM2255 automated rotary microtome (Leica Biosystems, Nussloch, Germany) with glass knives, and stained with toluidine blue and basic fuchsin. Sections were observed using an Olympus BX50F light microscope (Olympus Europa, Hamburg, Germany). The thickness of the leaf, mesophyll, palisade and spongy parenchyma was measured using the NIS-Elements AR 3.0 image analysis software (Laboratory Imaging, Prague, Czech Republic). Leaf density was calculated as the ratio between LMA and leaf thickness (Ďurkovič et al., 2012). Measurements were performed on two sun leaves per plant, one section per leaf, two measurements per section (both left side and right side from the leaf midrib). The experiments were repeated twice.

2.4. Gas exchange

An open portable photosynthesis system with infra-red gas analyser LI-6400 XT (LI-COR) was used for in situ gas exchange measurements. Net photosynthetic rate (P_N), transpiration (E), stomatal conductance (g_s) and internal-to-ambient CO_2 concentration ratio (C_i/C_a) were measured under a saturating photosynthetic photon flux density of 1200 ± 1 μmol m^{-2} s^{-1} and an ambient CO_2 concentration of 370 ± 1 μmol mol^{-1} using the 6400-08 standard leaf chamber with the 6400-02B red/blue LED light source (LI-COR). Instantaneous water-use efficiency (WUE_{inst}) was calculated as the ratio of P_N to E (Campbell et al., 2005). During measurements, microclimatic conditions inside the assimilation chamber were kept constant (leaf temperature 21 ± 1 °C, relative air humidity 60 ± 5%). The vapour pressure deficit ranged from 0.8 to 1.2 kPa. Measurements were performed on three sun leaves per plant, six measurements per leaf. Gas exchange parameters were averaged to generate leaf means; individual means were calculated from the leaf means. The experiments were repeated twice.

2.5. Chlorophyll fluorescence and chlorophyll content

Chlorophyll *a* fluorescence yields were measured using a portable fluorometer Plant Efficiency Analyser (Hansatech

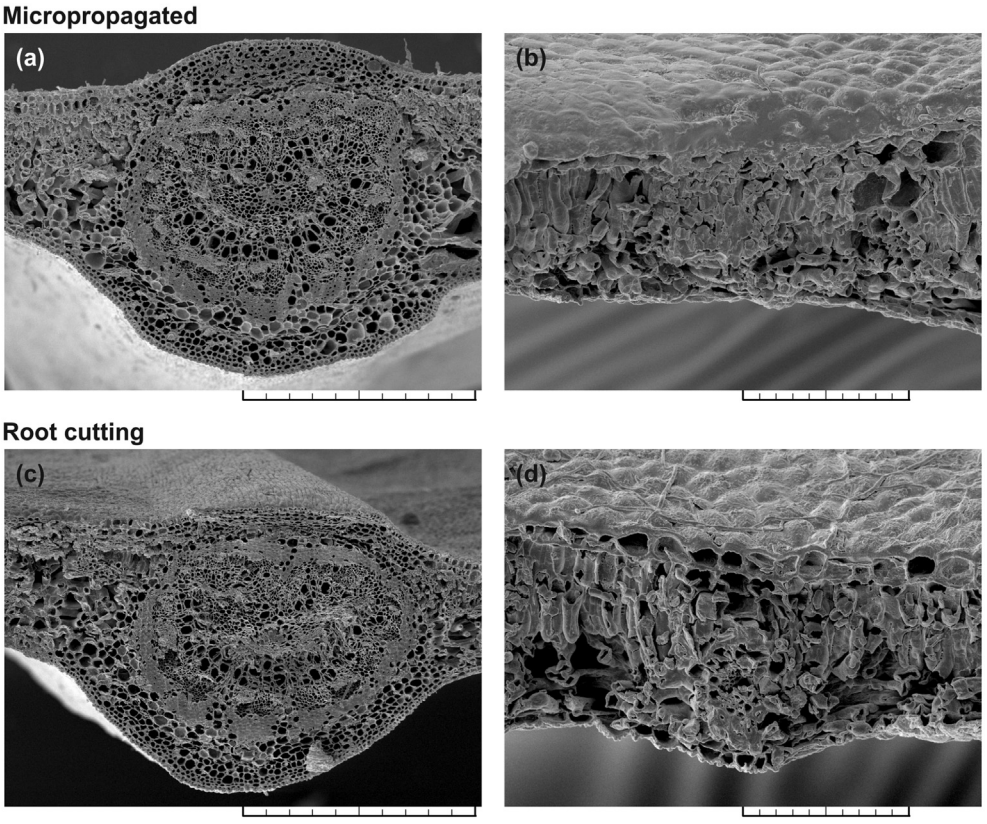

Fig. 1. Scanning electron microscopy images of leaf samples collected from the micropropagated plants and the plants propagated from root cuttings of the hybrid poplar T-14. (a, c) Leaf midrib and primary xylem area, cross-section. Scale bars = 500 μm. (b, d) Mesophyll tissue, cross-section. Scale bars = 100 μm.

Instruments Ltd. Kings Lynn, UK). Leaves were kept for 30 min under leaf clamps for dark adaptation. After the initial measurement of dark-adapted minimal fluorescence (F_0), leaves were exposed to a saturating irradiance of 2100 μmol m^{-2} s^{-1} for 1 s to measure the maximal fluorescence of dark-adapted foliage (F_m). Variable fluorescence (F_v) was calculated as $F_v = F_m - F_0$, and the parameters such as maximum photochemical efficiency of photosystem II (F_v/F_m), variable-to-initial fluorescence ratio (F_v/F_0) and potential electron acceptor capacity of photosystem II – "area" (i.e. area above the induction curve between F_0 and F_m) were determined. Measurements were performed on five sun leaves per plant, two measurements per leaf (one per adaxial surface and one per abaxial surface). The experiments were repeated twice.

Relative chlorophyll content was estimated with a portable chlorophyll meter CL-01 (Hansatech Instruments Ltd. Kings Lynn, UK) and the results were expressed as the chlorophyll index (Cassol et al., 2008). Measurements were performed on five sun leaves per plant, three measurements per adaxial leaf surface. Chlorophyll indices were averaged to generate leaf means; individual means were calculated from the leaf means. The experiments were repeated twice.

2.6. Leaf midrib vascular traits

Vascular characteristics of the leaf midrib primary xylem, i.e. tracheary element lumen area (A) and tracheary element densities (N) per 0.1 mm^2 of the primary xylem area, were determined using the NIS-Elements AR 3.0 image analysis software (Laboratory Imaging). The additional indicators of vascular strategy such as tracheary element lumen fraction ($F = A \times N$) and the tracheary element size: number ratio ($S = A/N$) were calculated as described by Zanne et al. (2010). Theoretical midrib hydraulic axial conductivity (K_t) per unit area (0.1 mm^2 of the primary xylem area) was calculated as the sum of hydraulic conductivities for each tracheary element divided by the area of a cross-section of primary xylem and multiplied by 0.1, whereas the individual K_t was calculated according to the following equation:

$$K_t = \frac{\pi a^3 b^3}{64\eta(a^2 + b^2)}$$

where a and b are the long and short axes of a tracheary element elliptical lumen and η is the viscosity of water at 20 °C (Dunbar-Co et al., 2009; Sack and Frole, 2006). To compare the examined stock types for midrib xylem supply capacity per leaf area, we calculated an area- and length-normalized theoretical hydraulic axial conductivity (K_t') by dividing total K_t by leaf area and leaf length (Dunbar-Co et al., 2009; Ďurkovič et al., 2012). Lignin autofluorescence in cell walls of tracheary elements was detected by excitation at 360 nm using a barrier filter with a transmission cut-off at 470 nm, and photographed using a Leica DM4000 B microscope equipped with a Leica DFC490 digital color CCD camera (Leica Microsystems, Wetzlar, Germany). Measurements were performed on two sun leaves per plant, one section per leaf midrib, one measurement per section. Tracheary element lumen areas were averaged to generate leaf means; individual means were calculated from the leaf means. The experiments were repeated twice.

2.7. Cell wall nanomechanics

Midrib sections (0.4 × 0.4 cm), excised from the leaf base, were fixed in 5% (v/v) glutaraldehyde in a 0.1 M cacodylate buffer at pH 7.0, dehydrated through a gradient series of ethanol, cleared with xylene, and embedded in paraffin as described by Ďurkovič and Mišalová (2009). Cross-sections, approximately 15 μm thick, were cut using a Bright Series 8000 retracting base sledge microtome (Bright Instruments, Luton, UK), deparaffinized in xylene, mounted on circle glass slides (11 mm in diameter) coated with (3-aminopropyl)triethoxy-silane, and allowed to air dry in sterile Petri dishes. PeakForce QNM measurements were done using a MultiMode 8 atomic force microscope with a Nanoscope V controller (Bruker Nano Surfaces, Santa Barbara, CA, USA). Cell walls of tracheary elements were tapped by a silicon cantilever MPP-13120, model TAP525A (Bruker AFM Probes, Camarillo, CA, USA) with a spring constant of 134.8 N m^{-1}, deflection sensitivity of 51.7 nm V^{-1}, and resonance frequency of 519.9 kHz, at 25 °C and ambient air pressure. Prior to each measurement, the actual tip end radius and geometry were controlled using a commercial TGT1 test grating (NT-MDT, Zelenograd, Russia) for 3-D visualization of the scanning tip. PeakForce QNM measurements of the reduced Young's MOE, adhesion, deformation and dissipation energy were performed at low approach tip velocities of 0.56–0.64 μm s^{-1}. To achieve accurate and reliable calculations of MOE, a sufficient sample deformation of at least 2 nm was ensured by adjusting the peak force setpoint to 165 nN. Measurements were performed on two sun leaves per plant, one tracheary element per leaf midrib, one measurement per cell wall of a tracheary element. The experiments were repeated twice.

2.8. AFM data processing

The initial data of the reduced Young's MOE, coming from the PeakForce QNM mapping (represented by 256 × 256 matrices), were analysed by NanoScope Analysis software, version 1.40r2 (Bruker AXS, Santa Brabara, CA, USA), which uses the Derjaguin-Muller-Toporov (DMT) model (Derjaguin et al., 1975). For the calculation of MOE, the DMT model accounts for adhesion by fitting the retract curve close to the contact point according to the following equation:

$$F_{TIP} - F_{ADH} = \frac{4}{3}\mathrm{MOE}\sqrt{R(d - d_0)^3}$$

where $F_{TIP} - F_{ADH}$ is the force on the tip cantilever relative to the adhesion force, R is the actual tip end radius, and $d - d_0$ is the deformation of the sample cell wall. The raw data of MOE were subsequently imported into the MATLAB software, version 7 (MathWorks, Natick, MA, USA), and the height gradient was calculated for each image pixel. Values corresponding to 'steep' points, where surface slope exceeded more than 20°, were not used (Ďurkovič et al., 2016).

2.9. Statistical analysis

Data were analysed by nested analysis of variance (plants were nested in stock types). The stock types were considered a fixed effect factor, whereas the plants were considered a random effect factor. The Pearson correlation coefficients were calculated for the selected trait–trait relationships. The correlations were considered significant if $P < 0.05$. Multivariate associations among leaf traits were analysed using a principal component analysis (PCA) to describe patterns of covariation among the growth, ecophysiological, vascular and nanomechanical traits (Quinn and Keough, 2002). Statistical analyses were performed in SAS/STAT 9.1 (SAS Institute, Cary, NC, USA).

3. Results and discussion

3.1. Leaf growth and gas exchange

The results of leaf growth traits are presented in Table 1. The techniques applied during vegetative propagation had a direct influence on leaf area, leaf length, leaf width and leaf dry mass. The micropropagated plants showed significantly higher values for these traits than those recorded for the plants propagated from root cuttings. For LMA, leaf slenderness, leaf density and the thickness of leaf tissues, however, non-significant differences were observed. In addition, a few of the gas exchange traits assessed varied with the applied propagation technique, namely E and WUE_{inst} (Table 2). The micropropagated plants reached a higher rate of E, whereas the performance of the plants propagated from root cuttings was superior for WUE_{inst}. A higher E explains the greater leaf area, leaf size dimensions and leaf dry mass in the micropropagated plants as there was no difference found for either leaf density or leaf thickness in the examined stock types. Recent studies suggest that the rate of transpiration is strongly determined by the hydraulic system within the entire plant. The differences in root hydraulic conductance through physiological functions of aquaporins contribute to the hydraulic conductance of the whole plant, and consequently to transpiration for the entire plant (Grondin et al., 2016; Meng and Fricke, 2017; Rodríguez-Gamir et al., 2016). Contrary to the in vitro micropropagated plants, their counterparts emerged directly from the mature root cuttings. We hypothesize that root hydraulic conductance and root water fluxes in the plants derived from root cuttings might differ from those in the micropropagated plants, resulting in a significant difference in the rate of transpiration found between the stock types.

Furthermore, no difference was observed for other gas exchange traits such as P_N, g_s, C_i/C_a or for chlorophyll index. This result is opposite to that found for the micropropagated plants of the Dutch elm hybrid 'Dodoens' (Ďurkovič et al., 2016). In that study, the authors found that the micropropagated plants reached significantly lower values of P_N, E and g_s than the grafted plants which were used as the counterparts for a comparison. Similar behaviour in gas exchange was also reported for micropropagated *Ulmus glabra* plants which similarly showed significantly lower values in P_N, E and g_s than the grafts (Ďurkovič et al., 2010). These results indicate that in vitro micropropagated plants are subjected to a greater degree of rejuvenation than are the grafts, and a greater rejuvenation in turn affects the stomatal regulation of photosynthesis in a more sensitive way. However, this was not the case in this research because the plants propagated from root cuttings showed very similar values of g_s and P_N to those of the micropropagated plants. Apparently, field performances in g_s and consequently in P_N for the plants propagated from root cuttings are quite different from those of the grafts. A relatedness in the vegetative plant origin between the plants derived from root cuttings and the micropropagated plants may explain why field performances in g_s and P_N were similar between the two stock types. Indeed, the measurements of g_s revealed that both the micropropagated plants and the plants propagated from root cuttings were subjected to a similar sensitivity in stomatal regulation of photosynthesis and transpiration. A higher g_s supported an increased carbon uptake during photosynthesis ($r = 0.95$, $P < 0.001$, Fig. 2a). Measurements of g_s explained 89% of the variation in P_N ($R^2 = 0.89$) indicating that a smaller proportion in variation was left for the non-stomatal component of photosynthesis. A higher g_s also supported a higher rate of E ($r = 0.90$, $P < 0.001$, Fig. 2b), and measurements of g_s explained 81% of the variation in E ($R^2 = 0.81$). Previous studies have shown that g_s plays a pivotal role in predicting carbon and water exchange between the atmosphere and terrestrial plants (Lin et al., 2015; Orchard et al., 2010). Our results with hybrid poplar plants confirmed that stomatal behaviour was an important regulator of gas exchange for both the micropropagated plants and for the plants propagated from root cuttings.

In addition, instantaneous C_i/C_a was linked to several gas exchange traits. A higher C_i/C_a supported a higher rate of g_s ($r = 0.59$, $P = 0.016$, Fig. 3a), and measurements of C_i/C_a explained 35% of the variation in g_s ($R^2 = 0.35$). A higher C_i/C_a also supported a higher rate of E ($r = 0.52$, $P = 0.037$, Fig. 3b), and measurements of C_i/C_a explained 27% of the variation in E ($R^2 = 0.27$). Finally, C_i/C_a was negatively correlated with WUE_{inst} but this relationship was only marginally significant ($r = -0.49$, $P = 0.052$, Fig. 3c), and

Table 2
Gas exchange and chlorophyll index in the hybrid poplar T-14.

Trait	Plant origin		P-value
	Micropropagated	Root cutting	
P_N (μmol CO_2 m^{-2} s^{-1})	10.9 ± 0.4	10.7 ± 0.5	0.7637 NS
E (mmol H_2O m^{-2} s^{-1})	1.63 ± 0.06	1.46 ± 0.07	0.0090 **
g_s (mmol H_2O m^{-2} s^{-1})	173 ± 8	169 ± 11	0.6896 NS
C_i/C_a (10^{-2})	66.5 ± 0.6	65.5 ± 0.7	0.2176 NS
WUE_{inst} (μmol CO_2 $mmol^{-1}$ H_2O)	6.72 ± 0.15	7.37 ± 0.11	0.0001 ***
CHLI	7.99 ± 0.11	7.82 ± 0.11	0.1647 NS

P_N, net photosynthetic rate; E, transpiration; g_s, stomatal conductance; C_i/C_a, internal-to-ambient CO_2 concentration ratio; WUE_{inst}, instantaneous water-use efficiency; CHLI, chlorophyll index.
Data represent means ± SE. Statistical results are based on nested analysis of variance with significance denoted as ***$P < 0.001$, **$P < 0.01$, and non-significant (NS) differences, respectively.

Table 1
Leaf growth traits in the hybrid poplar T-14.

Trait	Plant origin		P-value
	Micropropagated	Root cutting	
Leaf area (cm^2)	17.5 ± 0.5	15.6 ± 0.5	0.0021 **
Leaf length (cm)	5.31 ± 0.08	5.02 ± 0.08	0.0023 **
Leaf width (cm)	4.74 ± 0.06	4.40 ± 0.08	0.0003 ***
Leaf slenderness (cm cm^{-1})	1.12 ± 0.01	1.15 ± 0.01	0.1544 NS
Leaf dry mass (mg)	104 ± 3	92 ± 4	0.0016 **
Leaf mass per area (g m^{-2})	59.0 ± 0.7	58.2 ± 0.6	0.0701 NS
Leaf density (g cm^{-3})	0.44 ± 0.01	0.43 ± 0.02	0.7055 NS
Leaf thickness (μm)	134 ± 3	134 ± 3	0.8945 NS
Mesophyll thickness (μm)	111 ± 3	111 ± 2	0.9621 NS
Palisade parenchyma thickness (μm)	63.6 ± 1.4	63.9 ± 1.4	0.8479 NS
Spongy parenchyma thickness (μm)	47.5 ± 1.6	47.0 ± 1.5	0.8275 NS

Data represent means ± SE. Statistical results are based on nested analysis of variance with significance denoted as ***$P < 0.001$, **$P < 0.01$, and non-significant (NS) differences, respectively.

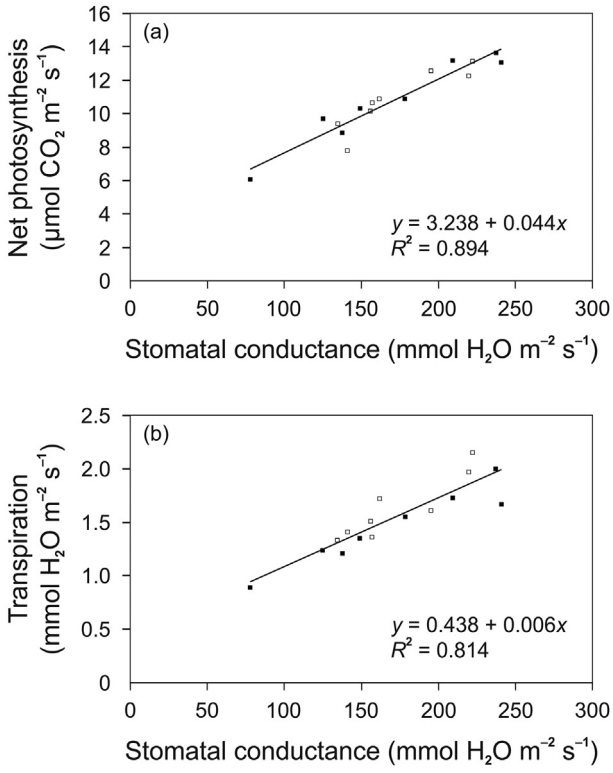

Fig. 2. Trait linkages with stomatal conductance (g_s) identified in the hybrid polar T-14. (a) Relationship of g_s to net photosynthetic rate. (b) Relationship of g_s to transpiration. Open squares show the micropropagated plants, filled squares show the plants propagated from root cuttings.

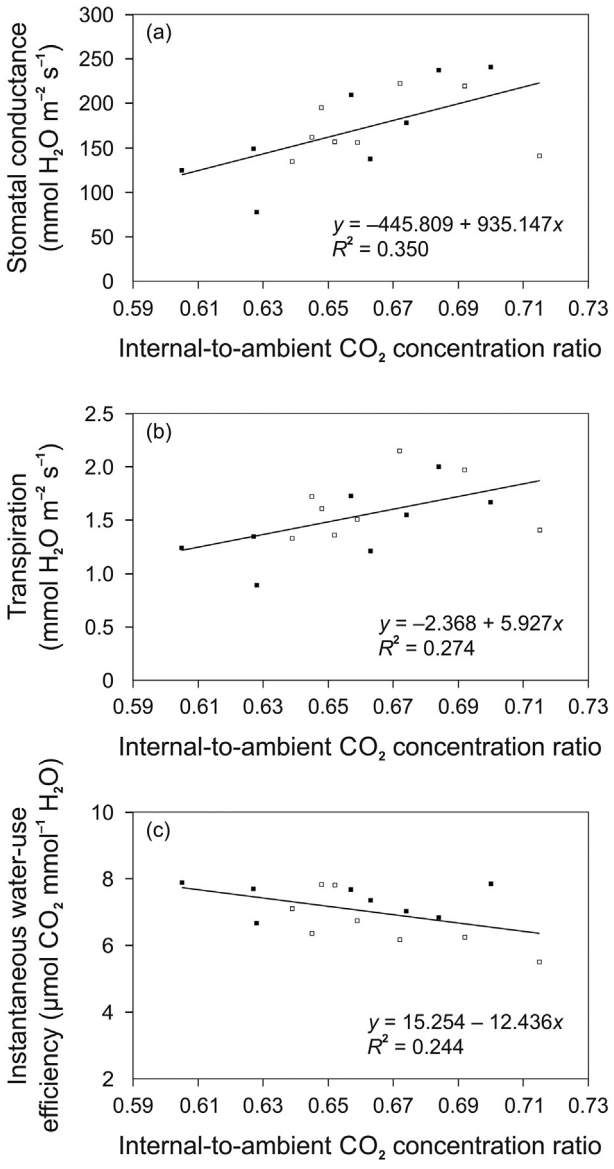

Fig. 3. Trait linkages with internal-to-ambient CO_2 concentration ratio (C_i/C_a) identified in the hybrid polar T-14. (a) Relationship of C_i/C_a to stomatal conductance. (b) Relationship of C_i/C_a to transpiration. (c) Relationship of C_i/C_a to instantaneous water-use efficiency. Open squares show the micropropagated plants, filled squares show the plants propagated from root cuttings.

measurements of C_i/C_a explained 24% of the variation in WUE_{inst} ($R^2 = 0.24$). In tropical trees, C_i/C_a has been found to be the primary determinant of WUE at the whole-plant level (Cernusak et al., 2007, 2009), and thus the measurements of instantaneous C_i/C_a are frequently employed as an indicator of variation in WUE. In this study, however, the relationship between these two variables was only marginally significant, probably due to a lack of variation in C_i/C_a between the stock types. Taken together, it could be assumed that due to a higher photosynthetic carbon gain per unit transpirational water vapour loss found in the plants propagated from root cuttings (Table 2), this stock type could have a higher acclimation capacity to stressful conditions during a severe drought than the micropropagated plants.

3.2. Chlorophyll a fluorescence yields

The micropropagated plants reached significantly higher values for F_v/F_m, F_v/F_0 and potential electron acceptor capacity than the plants propagated from root cuttings for both leaf surfaces (Table 3). For both stock types, there was no significant effect of the leaf surface on the F_v/F_m and F_v/F_0 ratios. For the variable "area", however, significantly higher values were recorded for adaxial than for abaxial surfaces. Typically, for nonstressed plants a characteristic F_v/F_m ratio of open photosystem II is in the range of 0.75–0.85. A rapid decline in F_v/F_m is a sensitive and early indicator of a change in photosynthesis and in the physiological status of the plant in general (Bolhàr-Nordenkampf et al., 1989). Measurements in this study revealed that the F_v/F_m ratio for the plants propagated from root cuttings reached an average value of 0.810 as opposed to 0.826 for the micropropagated plants. Thus, the reaction centers of photosystem II were functionally intact irrespective of the plant origin. Moreover, their F_v/F_m ratios were far higher than the threshold value of 0.725 which indicates the onset of reversible changes in the reaction centers of photosystem II (Čaňová et al., 2012). The variable F_v/F_0 estimates the maximum primary yield of photochemistry of photosystem II. A decline in F_v/F_0 ratio has been used as an indicator of drought stress (Li et al., 2006; Percival and Sheriffs, 2002). The variable "area" determines the potential acceptor capacity for electron transport during the primary processes of photosynthesis and has been shown to be a sensitive indicator of salinity (Panda et al., 2006). Despite lower values found in the plants propagated from root cuttings, chlorophyll *a* fluorescence yields were found within an optimum range for both nonstressed stock types. Under homogenous ecological site conditions, different behaviours of chlorophyll fluorescence characteristics were observed between early successional (light-demanding) and late successional (shade-tolerant) tree species (Pollastrini et al.,

Table 3
Chlorophyll *a* fluorescence in the hybrid poplar T-14.

Trait	Plant origin		*P*-value
	Micropropagated	Root cutting	
Adaxial surface			
F_v/F_m	0.826 ± 0.001	0.809 ± 0.003	0.0001 ***
F_v/F_0	4.71 ± 0.05	4.32 ± 0.07	0.0001 ***
"Area" (Mb s^{-1})	41.0 ± 0.9	34.0 ± 1.0	0.0001 ***
Abaxial surface			
F_v/F_m	0.826 ± 0.001	0.812 ± 0.002	0.0001 ***
F_v/F_0	4.76 ± 0.05	4.37 ± 0.07	0.0001 ***
"Area" (Mb s^{-1})	34.7 ± 0.8	28.0 ± 0.9	0.0001 **

F_v/F_m, maximum photochemical efficiency of photosystem II; F_v/F_0, variable-to-initial fluorescence ratio; "Area", potential electron acceptor capacity of photosystem II.
Data represent means ± SE. Statistical results are based on nested analysis of variance with significance denoted as ***$P < 0.001$.

2016; Sánchez-Gómez et al., 2006). But, on an intraclonal level, it remains unclear why the micropropagated plants had statistically higher chlorophyll *a* fluorescence yields than those of the plants propagated from root cuttings or those of the grafts as shown in previous studies (Ďurkovič et al., 2010, 2016). Also, the effect of in vitro physiological rejuvenation on chlorophyll fluorescence may be questionable. In a recent study, Nunes et al. (2016) did not observe any differences in chlorophyll *a* fluorescence parameters between in vitro micropropagated plants and ex vitro germinated seedlings of *Pinus elliottii*.

3.3. Vascular traits

The examined vegetative propagation techniques had no significant effect on leaf midrib vascular traits (Table 4). Differences between the micropropagated plants and the plants propagated from root cuttings were negligible for the traits such as *A*, *N*, *F*, *S*, K_t and K_t'. In both stock types, the water conducting area within the primary xylem tissue contained an equal number of equally-sized tracheary elements, which provided no functional advantage to either stock type in terms of hydraulic safety (when the vascular architecture, formed by a great number of small tracheary elements, is driven by embolism avoidance) or for a rapid and very effective water transport system (when the vascular architecture is formed by a small number of large tracheary elements) (Zanne and Falster, 2010). The relative amount of water transport space (measured by trait *F*), the variation in the vessel composition within the water transport space (assessed by trait *S*), as well as both theoretical hydraulic axial conductivities K_t and K_t' were similar for both stock types. This result is opposite to that found for the leaf midrib vascular traits of the Dutch elm hybrid 'Dodoens' (Ďurkovič et al., 2016). The authors found significant differences in the traits *N*, *F* and *S* between both the micropropagated plants and the grafts. The grafted elms had lower values of *N* and *F*, whereas the micropropagated elms had a lower value of *S*. This difference in leaf vascular performances was due to the rootstock used for grafting which often plays a role in the subsequent vascular growth of a scion. The effect of the rootstock was found to be responsible for the physiological alterations in water transport efficiencies and hydraulic conductance, e.g. in grafted *Malus domestica* (Cohen and Naor, 2002) or *Cucumis melo* plants (Agele and Cohen, 2009). In this research, however, the vascular performance of the micropropagated plants was similar to that of the plants propagated from root cuttings, and thus no disadvantage or compromise in the vascular architecture could be attributed to the micropropagated plants.

Table 4
Vascular traits in the hybrid poplar T-14.

Trait	Plant origin		*P*-value
	Micropropagated	Root cutting	
A (10^{-5} mm^2)	10.9 ± 0.2	11.0 ± 0.3	0.7931 NS
N (no./0.1 mm^2)	362 ± 6	365 ± 9	0.7173 NS
F (10^{-3} mm^2)	39.0 ± 0.4	39.4 ± 0.5	0.5048 NS
S (10^{-7} mm^4)	3.08 ± 0.11	3.13 ± 0.18	0.7763 NS
K_t (10^{-3} mmol m s^{-1} MPa^{-1})	15.0 ± 0.6	15.2 ± 0.6	0.7860 NS
K_t' (mmol m^{-2} s^{-1} MPa^{-1})	107 ± 14	143 ± 16	0.1170 NS

A, tracheary element lumen area; *N*, number of tracheary elements per 0.1 mm^2 of the primary xylem area; *F*, tracheary element lumen fraction; *S*, tracheary element size: number ratio; K_t, theoretical hydraulic axial conductivity per 0.1 mm^2 of the primary xylem area; K_t', theoretical hydraulic axial conductivity normalized by leaf area and length.
Data represent means ± SE. Statistical results are based on nested analysis of variance with non-significant (NS) differences.

In addition, the traits *A* and *N*, which are the primary indicators of vascular strategy, showed a significant negative correlation with each other ($r = -0.86$, $P < 0.001$, Fig. 4a), demonstrating a trade-off between the efficiency and the safety of water transport in the examined hybrid poplar stock types. Measurements of *N* explained 75% of the variation in *A* ($R^2 = 0.75$). Tracheary element lumen area strongly affects the capacity of xylem tissue to conduct water, whereas conduit density influences bulk xylem composition (Preston et al., 2006). The traits *A* and *N* were reported to be negatively correlated across angiosperms as well as gymnosperms (Sperry et al., 2008; Zanne et al., 2010).

3.4. Nanomechanical traits of tracherary element cell walls

The results of cell wall nanomechanics are given in Table 5.

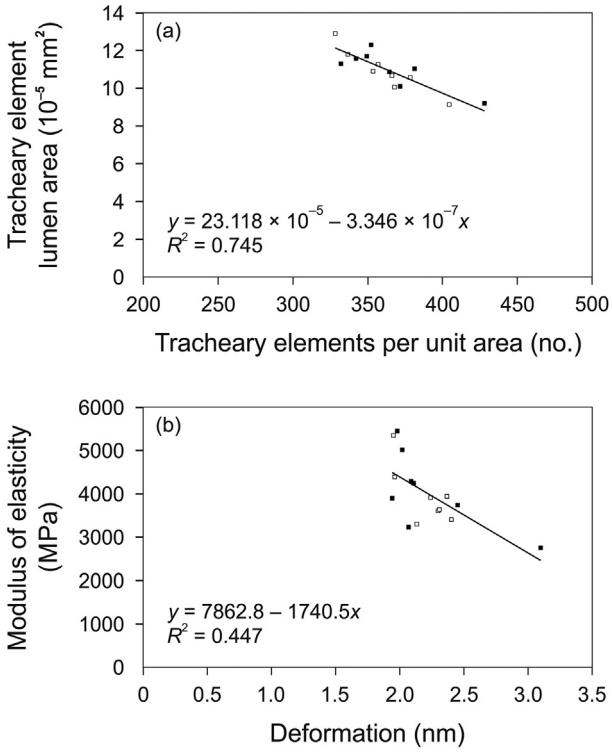

Fig. 4. Correlations of the number of tracheary elements per unit area of primary xylem (*N*) with tracheary element lumen area (*A*), and cell wall deformation with modulus of elasticity identified in the hybrid polar T-14. (a) Relationship of *N* to *A*. (b) Relationship of deformation to modulus of elasticity. Open squares show the micropropagated plants, filled squares show the plants propagated from root cuttings.

Table 5
Nanomechanical properties of tracheary element cell walls in the hybrid poplar T-14.

Trait	Plant origin		*P*-value
	Micropropagated	Root cutting	
Modulus of elasticity (MPa)	3942 ± 200	4078 ± 249	0.6491 NS
Adhesion (nN)	18.9 ± 0.8	17.5 ± 0.8	0.1740 NS
Deformation (nm)	2.21 ± 0.06	2.22 ± 0.10	0.9264 NS
Dissipation (eV)	2341 ± 182	1765 ± 176	0.0051 **

Data represent means ± SE. Statistical results are based on nested analysis of variance with significance denoted as $^{**}P < 0.01$, and non-significant (NS) differences, respectively.

Propagation techniques did not affect tracheary element cell wall stiffness quantified by MOE, nor adhesion and cell wall deformation because the differences were non-significant. In our previous study (Ďurkovič et al., 2016), we found that leaf midrib tracheary elements of the micropropagated Dutch elm hybrid 'Dodoens' plants had stiffer cell walls than those of the grafts. Alterations in the content and distribution of cell wall biopolymers between those two plant origins might be one of the major reasons for the differences found in MOE. In that case, the micropropagated plants might benefit directly from a higher MOE over the grafts by having a reduced risk of tracheary element implosion when an embolism spreads and cavitation of the water column occurs as a result of the stressful conditions produced by the causative agent of Dutch elm disease. In this research, however, the performance of the plants propagated from root cuttings matched exactly with those of the micropropagated plants for the above three nanomechanical traits. Table 5 shows that the only significant difference found was dissipation, i.e. the area in between approaching and retracting parts of the force-versus-separation curve, reflecting the energy dissipated between the tip and the sample during each tapping cycle. Dissipation can be strongly related to a mix of several factors including topography, elasticity, adhesion, and viscoelastic behaviour of a material. Dissipation energy follows a quadratic behaviour with respect to the adhesion force, thereby the relative increase of the adhesion force can explain the respective relative increase in dissipation energy to a large extent. Furthermore, the dissipation energy contains not only the adhesion energy between tip and surface but also the work for nonelastic sample deformation in contact, plus the work to finally release the tip gradually from the surface at increasing tip-sample distances after the point of maximum adhesion (Fischer et al., 2013). From a biomechanical viewpoint, an increased dissipation for tracheary element cell walls may indicate a higher nanoscale heterogeneity of cell wall constituents (Tai et al., 2007). Thus, for micropropagated plants subjected to abiotic stress conditions, the ability of the cell walls to absorb more energy suggests a higher damping capacity within the primary xylem tissue particularly for this stock type. In addition, both deformation and MOE showed a significant negative correlation with each other ($r = -0.67$, $P = 0.005$, Fig. 4b), and measurements of cell wall deformation explained 45% of the variation in MOE ($R^2 = 0.45$). The stiffer cell wall components (e.g., crystalline cellulose) show smaller deformations, suggesting a linear elastic material behaviour for the tracheary element cell wall as it is assumed in the AFM indentation models (Alméras et al., 2017; Clair and Thibaut, 2004).

The quantitative AFM imaging of tracheary element cell walls is shown in Fig. 5. These images show the structure of the cell wall

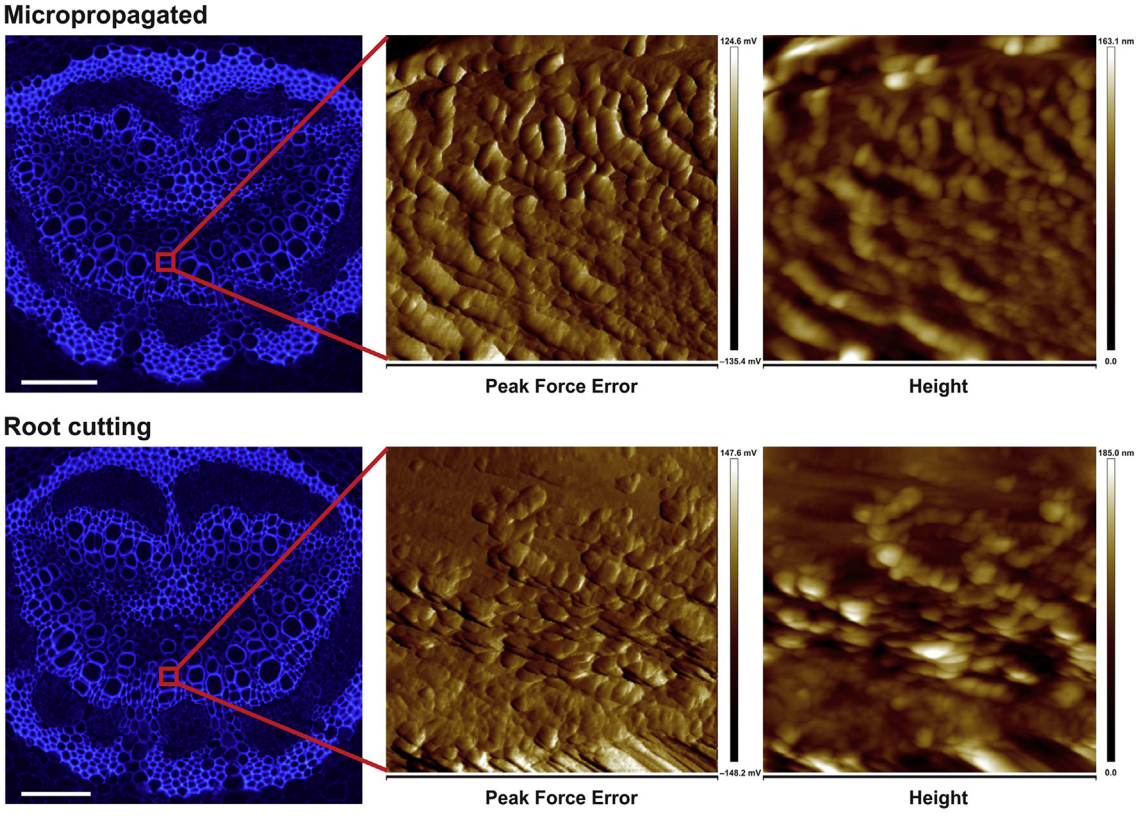

Fig. 5. Lignin autofluorescence images of primary xylem in the leaf midrib (left images), atomic force microscopy (AFM) peak force error images (middle images) and AFM flatten height images (right images) of neighbouring cell wall surfaces of the tracheary elements. Scale bars for the micropropagated plants of the hybrid poplar T-14: 50 μm for the fluorescence microscopy image, and 2.2 μm for AFM images. Scale bars for the plants propagated from root cuttings of the hybrid poplar T-14: 50 μm for the fluorescence microscopy image, and 2.0 μm for AFM images.

fragment surface in the peak force error and the height AFM channels. The peak force error channel produces a map of the peak force for each pixel in the image during the scan, and reveals the difference between the setpoint and the actual imaging force value. This error-signal provides a sensitive detection technique for the visualization of fine cell wall surface details. The height channel shows a height profile (i.e., cell wall topography).

3.5. Associations among leaf traits

A PCA was done to evaluate how the examined leaf traits were associated (Fig. 6). The first axis explained 29% of the variation and showed strong positive loadings for leaf area, leaf width, and chlorophyll *a* fluorescence parameters "area", F_v/F_0 and F_v/F_m. The negative side of the axis indicated strong loadings for P_N, g_s and chlorophyll index. The second axis explained 22% of the variation and showed strong positive loadings for LMA, *E* and leaf dry mass. The negative side of the axis indicated loadings for the vascular traits K_t', K_t and *A*, as well as for WUE_{inst}. The vector for LMA was nearly orthogonal to the K_t vector, thus demonstrating independence between these principal traits related to the leaf carbon economy and water flux (Sack and Holbrook, 2006). In addition, PCA showed that both plant origins formed compact homogeneous clusters separated from each other in the multivariate leaf trait analysis, except for the single outlier specimen from the group of the plants propagated from root cuttings. This specimen was positioned outside its own cluster, extending even beyond the cluster belonging to the micropropagated plants. Distributions of the micropropagated plants showed a lesser variation in the first PCA axis (which explained a major portion of the overall variation) and a greater variation in the second PCA axis. The plants propagated from root cuttings responded conversely, with great variation in the first PCA axis and lesser variation in the second PCA axis. A similar pattern for distributions of the leaf trait variation in the first and second PCA axes found here for the micropropagated hybrid poplar plants was also reported for the micropropagated plants of the Dutch elm hybrid 'Dodoens' (Ďurkovič et al., 2016). Both these studies, aimed at the leaf trait differences between various stock types, revealed that distributions of the micropropagated plants in the first PCA axis are more homogenous than those of the plants propagated from root cuttings or the grafted plants.

4. Conclusions

The results presented here illustrate that the techniques used for clonal propagation of the hybrid poplar clone T-14 affected the intraclonal variation of several leaf traits in both the micropropagated plants and the plants propagated from root cuttings. In the micropropagated plants, significantly greater leaf size dimensions resulted from the higher transpiration rate. The higher values of instantaneous water-use efficiency observed in the plants propagated from root cuttings indicate a higher acclimation

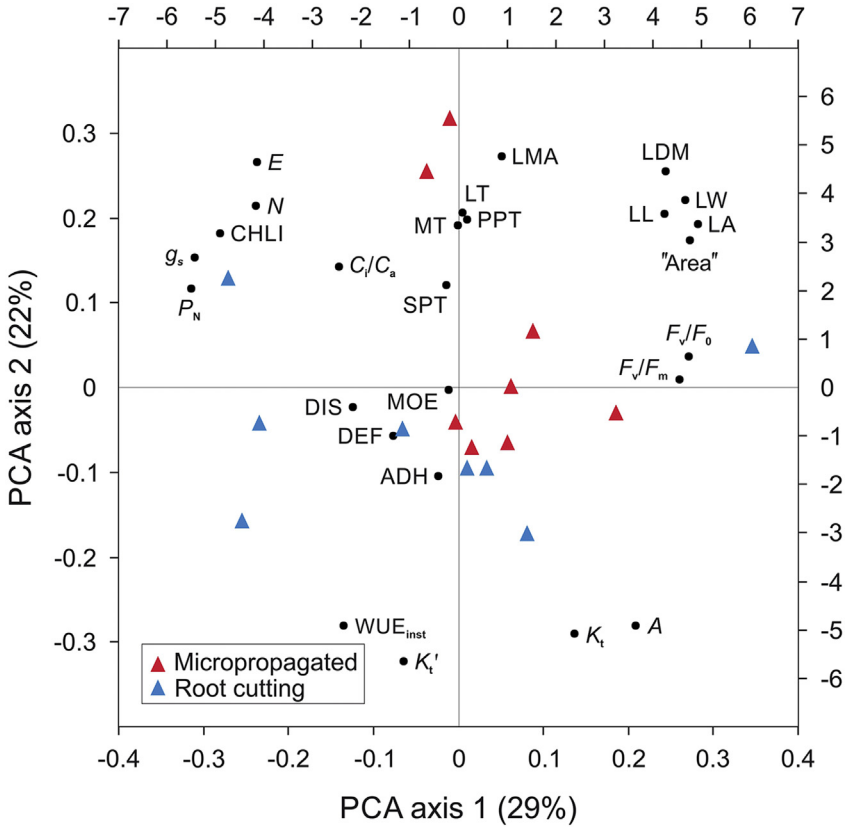

Fig. 6. Positions of leaf traits on the first and second axes of the principal component analysis (PCA). The bottom and left-hand axes refer to the examined leaf traits, whereas the top and right-hand axes refer to the examined trees. Trait abbreviations: *A*, tracheary element lumen area; ADH, adhesion; "Area", potential electron acceptor capacity of photosystem II; C_i/C_a, internal-to-ambient CO_2 concentration ratio; CHLI, chlorophyll index; DEF, deformation; DIS, dissipation energy; *E*, transpiration; F_v/F_m, maximum photochemical efficiency of photosystem II; F_v/F_0, variable-to-initial fluorescence ratio; g_s, stomatal conductance; K_t, theoretical hydraulic axial conductivity per 0.1 mm^2 of the primary xylem area; K_t', theoretical hydraulic axial conductivity normalized by leaf area and length; LA, leaf area; LDM, leaf dry mass; LL, leaf length; LMA, leaf mass per area; LT, leaf thickness; LW, leaf width; MOE, the reduced Young's modulus of elasticity; MT, mesophyll thickness; *N*, number of tracheary elements per 0.1 mm^2 of the primary xylem area; P_N, net photosynthetic rate; PPT, palisade parenchyma thickness; SPT, spongy parenchyma thickness; WUE_{inst}, instantaneous water-use efficiency. The micropropagated plants and the plants propagated from root cuttings of the hybrid poplar T-14 are as indicated in the key.

capacity to stressful conditions during a severe drought particularly for this stock type. Taken together, the micropropagated plants reached significantly higher values for 9 traits (30.0%), including leaf area, leaf size dimensions, leaf dry mass, *E*, chlorophyll *a* fluorescence parameters and the nanomechanical dissipation energy. There were no drawbacks in the leaf physiological performance which could be attributed to the micropropagated plants. The plants propagated from root cuttings reached a higher value for the single trait WUE_{inst} (3.3%). Similarities between the vegetative plant origins were found for 20 traits (66.7%), including g_s, P_N, indicators of leaf midrib vascular architecture, as well as for the majority of cell wall nanomechanical traits.

Contributions

Jaroslav Ďurkovič conceived and designed the experiment. Hana Husárová, Lucia Javoříková, Ingrid Čaňová, Miriama Šuleková, Monika Kardošová, Ivan Lukáčik and Miroslava Mamoňová performed the experiments. Jaroslav Ďurkovič and Rastislav Lagaňa analyzed the data. Ingrid Čaňová prepared the figures and Jaroslav Ďurkovič wrote the manuscript. All authors reviewed and approved the manuscript.

Acknowledgements

The authors thank Dr. D. Kurjak for his technical assistance with gas exchange measurements and Mrs. E. Ritch-Krč for language revision. This work was supported by funding from the Slovak scientific grant agency VEGA (1/0149/15).

References

Agele, S., Cohen, S., 2009. Effect of genotype and graft type on the hydraulic characteristics and water relations of grafted melon. J. Plant Interact. 4, 59–66.
Alméras, T., Gronvold, A., van der Lee, A., Clair, B., Montero, C., 2017. Contribution of cellulose to the moisture-dependent elastic behaviour of wood. Compos. Sci. Technol. 138, 151–160.
Arnould, O., Arinero, R., 2015. Towards a better understanding of wood cell wall characterisation with contact resonance atomic force microscopy. Compos. Part A Appl. Sci. Manuf. 74, 69–76.
Bojarczuk, K., Karliński, L., Hazubska-Przybył, T., Kieliszewska-Rokicka, B., 2015. Influence of mycorrhizal inoculation on growth of micropropagated *Populus* × *canescens* lines in metal-contaminated soils. New For. 46, 195–215.
Bolhàr-Nordenkampf, H.R., Long, S.P., Baker, N.R., Öquist, G., Schreiber, U., Lechner, E.G., 1989. Chlorophyll fluorescence as a probe of the photosynthetic competence of leaves in the field: a review of current instrumentation. Funct. Ecol. 3, 497–514.
Campbell, D.R., Galen, C., Wu, C.A., 2005. Ecophysiology of first and second generation hybrids in a natural plant hybrid zone. Oecologia 144, 214–225.
Cassol, D., De Silva, F.S.P., Falqueto, A.R., Bacarin, M.A., 2008. An evaluation of non-destructive methods to estimate total chlorophyll content. Photosynthetica 46, 634–636.
Čaňová, I., Ďurkovič, J., Hladká, D., Lukáčik, I., 2012. Changes in stomatal characteristics and photochemical efficiency during leaf development in six species of *Sorbus*. Photosynthetica 50, 635–640.
Cernusak, L.A., Winter, K., Aranda, J., Turner, B.L., Marshall, J.D., 2007. Transpiration efficiency of a tropical pioneer tree (*Ficus insipida*) in relation to soil fertility. J. Exp. Bot. 58, 3549–3566.
Cernusak, L.A., Winter, K., Aranda, J., Virgo, A., Garcia, M., 2009. Transpiration efficiency over an annual cycle, leaf gas exchange and wood carbon isotope ratio of three tropical tree species. Tree Physiol. 29, 1153–1161.
Clair, B., Thibaut, B., 2004. Evaluation of physical and mechanical properties at cell wall level with new microscopy tools. In: Schmitt, U., Ander, P., Barnett, J.R., Emons, A.M.C., Jeronimidis, G., Saranpää, P., Tschegg, S. (Eds.), Wood Fibre Cell Walls: Methods to Study Their Formation, Structure and Properties. COST Action E20. Swedish University of Agricultural Sciences, Uppsala, pp. 245–263.
Cohen, S., Naor, A., 2002. The effects of three rootstocks on water use, canopy conductance and hydraulic parameters of apple trees and predicting canopy from hydraulic conductance. Plant Cell Environ. 25, 17–28.
Derjaguin, B.V., Muller, V.M., Toporov, Y.P., 1975. Effect of contact deformations on the adhesion of particles. J. Colloid Interf. Sci. 53, 314–326.
Ding, D., Zhou, X., Ji, Z., You, T., Xu, F., 2016. How does hemicelluloses removal alter plant cell wall nanoscale architecture and correlate with enzymatic digestibility? Bioenerg. Res. 9, 601–609.
Dufrêne, Y.F., Martínez-Martín, D., Medalsy, I., Alsteens, D., Müller, D.J., 2013. Multiparametric imaging of biological systems by force-distance curve-based AFM. Nat. Methods 10, 847–854.
Dunbar-Co, S., Sporck, M.J., Sack, L., 2009. Leaf trait diversification and design in seven rare taxa of the Hawaiian *Plantago* radiation. Int. J. Plant Sci. 170, 61–75.
Ďurkovič, J., Mišalová, A., 2009. Wood formation during ex vitro acclimatisation in micropropagated true service tree (*Sorbus domestica* L.). Plant Cell Tissue Organ Cult. 96, 343–348.
Ďurkovič, J., Čaňová, I., Priwitzer, T., Biroščíková, M., Kapraľ, P., Saniga, M., 2010. Field assessment of photosynthetic characteristics in micropropagated and grafted wych elm (*Ulmus glabra* Huds.) trees. Plant Cell Tissue Organ Cult. 101, 221–228.
Ďurkovič, J., Kardošová, M., Čaňová, I., Lagaňa, R., Priwitzer, T., Chorvát Jr., D., Cicák, A., Pichler, V., 2012. Leaf traits in parental and hybrid species of *Sorbus* (Rosaceae). Am. J. Bot. 99, 1489–1500.
Ďurkovič, J., Kaňuchová, A., Kačík, F., Mamoňová, M., Lengyelová, A., 2013. Wood ontogeny during the first year of hybrid poplar development. Biol. Plant. 57, 591–596.
Ďurkovič, J., Čaňová, I., Kardošová, M., Kurjak, D., 2014. Seasonal patterns of leaf photosynthetic and secondary xylem vascular traits in current-year stems of three *Sorbus* species with contrasting growth habits. Plant Biol. 16, 908–916.
Ďurkovič, J., Čaňová, I., Javoříková, L., Kardošová, M., Lagaňa, R., Priwitzer, T., Longauer, R., Krajňáková, J., 2016. The effects of propagation techniques on leaf vascular anatomy, modulus of elasticity, and photosynthetic traits in micropropagated and grafted plants of the Dutch elm hybrid 'Dodoens'. J. Am. Soc. Hortic. Sci. 141, 351–362.
Eder, M., Arnould, O., Dunlop, J.W.C., Hornatowska, J., Salmén, L., 2013. Experimental micromechanical characterisation of wood cell walls. Wood Sci. Technol. 47, 163–182.
Fischer, H., Stadler, H., Erina, N., 2013. Quantitative temperature-depending mapping of mechanical properties of bitumen at the nanoscale using the AFM operated with PeakForce Tapping™ mode. J. Microsc. 250, 210–217.
Gindl, W., Gupta, H.S., Schöberl, T., Lichtenegger, H.C., Fratzl, P., 2004. Mechanical properties of spruce wood cell walls by nanoindentation. Appl. Phys. A 79, 2069–2073.
Grondin, A., Mauleon, R., Vadez, V., Henry, A., 2016. Root aquaporins contribute to whole plant water fluxes under drought stress in rice (*Oryza sativa* L.). Plant Cell Environ. 39, 347–365.
Hazarika, B.N., 2006. Morpho-physiological disorders in in vitro culture of plants. Sci. Hortic. 108, 105–120.
Janmey, P.A., Winer, J.P., Murray, M.E., Wen, Q., 2009. The hard life of soft cells. Cell Motil. Cytoskeleton 66, 597–605.
Kačík, F., Ďurkovič, J., Kačíková, D., 2012. Chemical profiles of wood components of poplar clones for their energy utilization. Energies 5, 5243–5256.
Kaňuchová, A., Ďurkovič, J., 2013. Wood ontogeny during ex vitro acclimatization in micropropagated hybrid poplar clones. Biol. Plant. 57, 144–148.
Kirova, M., Ceppi, G., Chernev, P., Goltsev, V., Strasser, R., 2009. Using artificial neural networks for plant taxonomic determination based on chlorophyll fluorescence induction curves. Biotechnol. Biotechnol. Equip. 23S, 941–945.
Kučerová, V., Výbohová, E., Čaňová, I., Ďurkovič, J., 2016. The effects of both insoluble lignin and the macromolecular traits of cellulose on the content of saccharides within solids during hydrothermal pretreatment of hybrid poplar wood. Ind. Crops Prod. 91, 22–31.
Li, R.-h., Guo, P.-g., Baum, M., Grando, S., Ceccarelli, S., 2006. Evaluation of chlorophyll content and fluorescence parameters as indicators of drought tolerance in barley. Agric. Sci. China 5, 751–757.
Lin, Y.-S., Medlyn, B.E., Duursma, R.A., Prentice, I.C., Wang, H., Baig, S., Eamus, D., de Dios, V.R., Mitchell, P., Ellsworth, D.S., de Beeck, M.O., Wallin, G., Uddling, J., Tarvainen, L., Linderson, M.-L., Cernusak, L.A., Nippert, J.B., Ocheltree, T.W., Tissue, D.T., Martin-StPaul, N.K., Rogers, A., Warren, J.M., De Angelis, P., Hikosaka, K., Han, Q., Onoda, Y., Gimeno, T.E., Barton, C.V.M., Bennie, J., Bonal, D., Bosc, A., Löw, M., Macinins-Ng, C., Rey, A., Rowland, L., Setterfield, S.A., Tausz-Posch, S., Zaragoza-Castells, J., Broadmeadow, M.S.J., Drake, J.E., Freeman, M., Ghannoum, O., Hutley, L.B., Kelly, J.W., Kikuzawa, K., Kolari, P., Koyama, K., Limousin, J.-M., Meir, P., da Costa, A.C.L., Mikkelsen, T.N., Salinas, N., Sun, W., Wingate, L., 2015. Optimal stomatal behaviour around the world. Nat. Clim. Change 5, 459–464.
Meng, D., Fricke, W., 2017. Changes in root hydraulic conductivity facilitate the overall hydraulic response of rice (*Oryza sativa* L.) cultivars to salt and osmotic stress. Plant Physiol. Biochem. 113, 64–77.
Nunes, S., Santos, C., Moutinho-Pereira, J., Correia, C., Oliveira, H., Ferreira de Oliveira, J.M., Pereira, V.T., Almeida, T., Marum, L., Dias, M.C., 2016. Physiological characterization and true-to-typeness evaluation of in vitro and ex vitro seedlings of *Pinus elliottii*: a contribution to breedings programs. Plant Physiol. Biochem. 107, 222–227.
Orchard, K.A., Cernusak, L.A., Hutley, L.B., 2010. Photosynthesis and water-use efficiency of seedlings from northern Australian monsoon forest, savanna and swamp habitats grown in a common garden. Funct. Plant Biol. 37, 1050–1060.
Osório, M.L., Osório, J., Gonçalves, S., David, M.M., Correia, M.J., Romano, A., 2012. Carob trees (*Ceratonia siliqua* L.) regenerated in vitro can acclimatize successfully to match the field performance of seed-derived plants. Trees 26, 1837–1846.
Osório, M.L., Gonçalves, S., Coelho, N., Osório, J., Romano, A., 2013. Morphological, physiological and oxidative stress markers during acclimatization and field transfer of micropropagated *Tuberaria major* plants. Plant Cell Tissue Organ Cult. 115, 85–97.
Panda, D., Dash, P.K., Dhal, N.K., Rout, N.C., 2006. Chlorophyll fluorescence

parameters and chlorophyll content in mangrove species grown in different salinity. Gen. Appl. Plant Physiol. 32, 175–180.
Percival, G.C., Sheriffs, C.N., 2002. Identification of drought-tolerant woody perennials using chlorophyll fluorescence. J. Arboric. 28, 215–223.
Pollastrini, M., Holland, V., Brüggemann, W., Bruelheide, H., Dănilă, I., Jaroszewicz, B., Valladares, F., Bussotti, F., 2016. Taxonomic and ecological relevance of the chlorophyll *a* fluorescence signature of tree species in mixed European forests. New Phytol. 212, 51–65.
Preston, K.A., Cornwell, W.K., DeNoyer, J.L., 2006. Wood density and vessel traits as distinct correlates of ecological strategy in 51 California coast range angiosperms. New Phytol. 170, 807–818.
Quinn, G.P., Keough, M.J., 2002. Experimental Design and Data Analysis for Biologists. Cambridge University Press, Cambridge.
Quinn, L.D., Straker, K.C., Guo, J., Kim, S., Thapa, S., Kling, G., Lee, D.K., Voigt, T.B., 2015. Stress-tolerant feedstocks for sustainable bioenergy production on marginal land. Bioenerg. Res. 8, 1081–1100.
Ren, D., Wang, H., Yu, Z., Wang, H., Yu, Y., 2015. Mechanical imaging of bamboo fiber cell walls and their composites by means of peakforce quantitative nanomechanics (PQNM) technique. Holzforschung 69, 975–984.
Rodríguez-Gamir, J., Primo-Millo, E., Forner-Giner, M.A., 2016. An integrated view of whole-tree hydraulic architecture. Does stomatal or hydraulic conductance determine whole tree transpiration? PLoS One 11, e0155246.
Sack, L., Frole, K., 2006. Leaf structural diversity is related to hydraulic capacity in tropical rain forest trees. Ecology 87, 483–491.
Sack, L., Holbrook, N.M., 2006. Leaf hydraulics. Annu. Rev. Plant Biol. 57, 361–381.
Salvatori, E., Fusaro, L., Gottardini, E., Pollastrini, M., Goltsev, V., Strasser, R.J., Bussotti, F., 2014. Plant stress analysis: application of prompt, delayed chlorophyll fluorescence and 820 nm modulated reflectance. Insights from independent experiments. Plant Physiol. Biochem. 85, 105–113.
Sánchez-Gómez, D., Valladares, F., Zavala, M.A., 2006. Functional traits and plasticity in response to light in seedlings of four Iberian forest tree species. Tree Physiol. 26, 1425–1433.
Sannigrahi, P., Ragauskas, A.J., 2010. Poplar as a feedstock for biofuels: a review of compositional characteristics. Biofuels Bioprod. Biorefin. 4, 209–226.
Savitch, L.V., Massacci, A., Gray, G.R., Huner, N.P.A., 2000. Acclimation to low temperature or high light mitigates sensitivity to photoinhibition: roles of the Calvin cycle and the Mehler reaction. Aust. J. Plant Physiol. 27, 253–264.
Sperry, J.S., Meinzer, F.C., McCulloh, K.A., 2008. Safety and efficiency conflicts in hydraulic architecture: scaling from tissues to trees. Plant Cell Environ. 31, 632–645.
Stolarski, M.J., Krzyżaniak, M., Łuczyński, M., Załuski, D., Szczukowski, S., Tworkowski, J., Gołaszewski, J., 2015. Lignocellulosic biomass from short rotation woody crops as a feedstock for second-generation bioethanol production. Ind. Crops Prod. 75, 66–75.
Tai, K., Dao, M., Suresh, S., Palazoglu, A., Ortiz, C., 2007. Nanoscale heterogeneity promotes energy dissipation in bone. Nat. Mater. 6, 454–462.
Zanne, A.E., Falster, D.S., 2010. Plant functional traits – linkages among stem anatomy, plant performance and life history. New Phytol. 185, 348–351.
Zanne, A.E., Westoby, M., Falster, D.S., Ackerly, D.D., Loarie, S.R., Arnold, S.E.J., Coomes, D.A., 2010. Angiosperm wood structure: global patterns in vessel anatomy and their relation to wood density and potential conductivity. Am. J. Bot. 97, 207–215.
Zemleduch-Barylska, A., Lorenc-Plucińska, G., 2015. *Populus* × *canescens* grown on Cr-rich tannery waste: comparison of leaf and root biochemical and proteomic responses. Plant Physiol. Biochem. 90, 1–13.
Zhou, X., Ma, J., Ji, Z., Zhang, X., Ramaswamy, S., Xu, F., Sun, R.-c, 2014. Dilute acid pretreatment differentially affects the compositional and architectural features of *Pinus bungeana* Zucc. compression and opposite wood tracheid walls. Ind. Crops Prod. 62, 196–203.